Separation and Purification Technology 283 (2022) 120201

Contents lists available at ScienceDirect

Separation and Purification Technology

journal homepage: www.elsevier.com/locate/seppur

In situ Assembly of Functionalized Single-Walled Carbon Nanotube with partially reduced Graphene oxide Nanocomposite Membrane for Chiral Separation of β-substituted-α-amino acids

Monti Gogoi, Rajiv Goswami, Alimpia Borah, Swapnali Hazarika *

Chemical Engineering Group, Engineering Sciences & Technology Division, CSIR-North East Institute of Science and Technology, Jorhat 785006, Assam, India
Academy of Scientific and Innovative Research (AcSIR), Ghaziabad 201002, India

ARTICLE INFO

Keywords:
rGO
Carbon Nanotube
Interfacial polymerization
Nanofiltration
Chiral Membrane

ABSTRACT

The usage of functionalized nanoporous materials with a high aspect ratio, excellent selectivity, good thermal and chemical robustness and easy aqueous processability can significantly influence the membrane-based chiral separation process. In the present study, we have reported a tunable pillar of rGO-FSWCNT based nanocomposite membrane for the chiral separation of β-substituted-α-amino acids. The nanocomposite membranes were prepared via Interfacial Polymerization (IP) method between partially rGO-FSWCNT composite and trimesoylchloride over the surface of polysulfone support. The membrane permeation experiment investigated the influence of physicochemical factors such as permeation time, operating pressure, and feed concentration on the separation performance. Nanocomposite membranes containing D-tryptophan as the chiral probe preferentially adsorbed the D-isomer of the racemic mixture while allowing the passage of the L-isomer to the permeate side. A maximum of 88–99.4 % of $ee_{(L)-isomer}$ was obtained for each racemic mixture separated under optimal experimental parameters such as feed concentration of the racemic mixture of 10 mmol.L^{-1}, an applied pressure of 3.5 bar, a flow rate of 25 mL.min^{-1} and a temperature of 25 °C. The pillaring effect exhibited by vertically aligned CNT within graphene planes possesses desirable L-isomer transport and provide excellent mechanical properties to retentate the D-isomer over nanocomposite membrane. This effect has proven that the synergistic assembly of FSWCNT acts as chiral probe to successfully fabricate the pillared tunnel for better enantioseparation of chiral molecules.

1. Introduction

In the field of drug design and development, synergistic relationship amid chirality and pharmacological action of drug molecules is inevitable, which demands the synthesis of drug molecules in their highest enantiopure forms [1]. The synthesis of drug molecules based on the enantioselective way is impractical either because of low yield or high expenditure of the synthesis process; chiral separation of a racemate is a superior alternative to afford the desired enantiopure product [2,3]. To date, different chiral resolution techniques such as enzymatic resolution [4], crystallization [5], and chromatographic separation [6] have been widely employed to achieve the enantio-selective separation of racemic mixtures. Recently it has been demonstrated that the nanoporous membrane systems can also be utilized as an excellent platform to achieve bulk scale separation of chiral molecules [7]. In a nanoporous membrane matrix, the feed racemates have only one choice of event, either they will pass through the nanopore or get adsorbed onto the pore, rather than undergoing a number of chemical interactions with stationary phase as anticipated from conventional chiral chromatographic techniques. So the result is a seamless permeate flux which facilitates macroscopic separation of a racemic mixture. Nevertheless, a nanopore cannot stand alone as an operative tool to discriminate between the enantiomers. A gatekeeper molecule is incorporated into the nanopore rim to realize the chiral environment, often called the chiral probe. The D and L isomer show different binding affinities towards the chiral probe leading to a difference in binding energy. The binding energy difference is further amplified by pre-organization of the racemate dimers around the nanoporous cavity leading to the adsorption of one

* Corresponding author at: Chemical Engineering Group, Engineering Sciences & Technology Division, CSIR-North East Institute of Science and Technology, Jorhat 785006, Assam, India.
E-mail address: shrrljt@yahoo.com (S. Hazarika).

https://doi.org/10.1016/j.seppur.2021.120201
Received 11 October 2021; Received in revised form 15 November 2021; Accepted 22 November 2021
Available online 27 November 2021

isomer onto the chiral probe while the other to pass through the nanoporous matrix [8].

Nanoporous membrane-assisted chiral separation techniques, especially those fabricated from carbonaceous nanomaterials, are gaining tremendous attention owing to their high chemical and thermal stability, excellent selectivity with decent permeability, antifouling properties, etc. However, the efficiency of a membrane system is defined in terms of membrane permeability and perm-selectivity parameters [9]. Unfortunately, most membranes that obey facilitated transport mechanisms are subjected to a trade-off between permeability and selectivity. Consequently, the main aim of preparing a mixed matrix membrane is to resolve enantiomers for simultaneously maximizing both permeability and permselectivity for enantiomers [10,11]. In this regard, membranes involving retarded mechanism during transport of molecules have the capability to balance this trade-off and lots of attention has been paid to fabricate functional membranes out of carbonaceous materials such as Graphene oxide (GO) [12], graphitic carbon nitride (g-C_3N_4) [13], carbon nanotube (CNT) [14,15], etc. for highly efficient chiral separation. Notably, adding a chiral selector to functionalize GO sheets has been confirmed to exhibit enantioselective performances toward enantiomeric target guests. The 2D membrane fabricated via reconstruction of the corresponding exfoliated colloidal dispersions creates numerous sub-nanometer channels that render excellent selectivity to the overall separation process [12]. However, the sub-nanometric channels that confer unprecedented selectivity also restricted the ultrafast permeation of solvents. So solvent dynamics is strategically adjusted via different techniques such as varying the size of the lateral sheet of GO in the reconstructed membrane to acquired desired permeation and selectivity [16] or molecules (or ion) sandwiching between adjacent layers, that can exhibit dramatic effect tortuous paths and transport properties of the lamellar membranes [17]. In such a hybrid membrane matrix, the impregmentation ratio of a chiral selector to spacer plays a critical role in evaluating the overall membrane performance [18]. Therefore, a contradiction was encountered in GO-based mixed matrix membranes because of enhancing the chiral selectors and controlling the efficient interlayer spacing [12]. To overcome this issue, we have adopted a facile strategy to enhance GO membrane's selectivity and permittivity via intercalating a functionalized single-walled carbon nanotubes (FSWCNTs), which will act both as a spacer as well as chiral selector.

In general, epoxides are oxygen ring containing functional groups present in GO. Therefore, their degree of functionalization (DF) can be conveniently maintained through amination reaction, by which ring opening of epoxide occurs [12,18]. Previously, for the first time, our group reported a functionalized single-walled carbon nanotubes (FSWCNT) thin-film membrane with D-Tryptophan as a chiral probe for the separation of tyrosine racemates [14]. Accordingly, these results accelerated us to introduce FSWCNT within the basal plane of GO. Herein, we reported that the FSWCNT, in reduced Graphene Oxide – Functionalized Single-walled Carbon Nanotubes (rGO-FSWCNT) hybrid system plays two different roles in the chiral resolution: i) behaves as spacer to exfoliate the stacked interlayer of GO based membrane and therefore, can achieve high throughput of enantiomer; ii) as an effective reactive site to induce the increase in grafting amount of D-tryptophan and to facilitate the transport of particular enantiomers.

The objective of this research work is to develop a rational strategy for the extension of the unique properties of covalently functionalized FSWCNT and graphene and study its application in chiral separation. Here, we have verified this speculation by examining the enantioseparation performance of rGO-FSWCNTs membranes for β-substituted-α-amino acids. Firstly, GO sheets were prepared using modified Hummers' method followed by the synthesis of a new composite of rGO-FSWCNT and fabrication of this material in the PSf support. Afterward, separation performances of rGO-FSWCNT based membranes for chiral isomers were studied. The obtained results have indicated that rGO-FSWCNT based membranes exhibited a noticeable improvement during the chiral separation of various β-substituted-α-amino acids such as 3,4-dihydroxyphenylalanine, 1-methyltryptophan, Tryptophan, Threonine and Tyrosine.

2. Experiment section

2.1. Materials

M/s Sisco Research Laboratory Pvt. Ltd (SRL), Mumbai, India provided Polyethylene Glycol (PEG). Polysulfone of 30,000 molecular weight were purchased from M/s SIGMA-Aldrich.M/s RANKEM range of laboratory chemicals, Gujarat, India supplied hydrazine hydrate (H_6N_2O), graphene flakes, DL-, D- and L-3,4-dihydroxyphenylalanine/ DOPA ($C_9H_{11}NO_4$), 1-methyltryptophan ($C_{12}H_{14}N_2O_2$), Tryptophan ($C_{11}H_{12}N_2O_2$), Threonine ($C_4H_9NO_3$) Tyrosine ($C_9H_{11}NO_3$) and 1,3,5-Benzenetricarboxylic acid chloride/ Trimesoylchloride/TMC ($C_9H_3Cl_3O_3$). Oxidizing agent Hydrogen Peroxide (H_2O_2) and Sulphuric acid (H_2SO_4), Ethanol (C_2H_5OH), Hydrochloric acid (HCl), n-Hexane (C_6H_{14}) and N-methyl pyrrolidine (NMP). M/s TCI Chemicals provided phosphoric acid (H_3PO_4) and Potassium permanganate ($KMnO_4$).

2.2. Preparation of graphene oxide (GO)

Modified Hummer's method was used to prepare Graphene oxide [19]. This process was initiated by an 8:1 mixture of concentrated H_2SO_4 followed by H_3PO_4. In a reaction vessel, 4 gm (1 wt equiv.) of graphite flakes was mixed with 20 gm (5 wt% equiv.) of $KMnO_4$, and the mixture was strongly agitated for 14 h at 45 °C. Afterward, it was cooled at 25 °C and then the reaction mixture was kept in an ice bath under continuous stirring. The mixture was further diluted to 500 mL through the addition of deionized water, followed by 2.5 mL of 25 % H_2O_2. To separate the solid residue from solution mixture, centrifugation of the mixture was carried out at 4500 rpm. The remaining residue was washed successively with 300 mL of water and 6 % of 300 mL HCl. The excess of $KMnO_4$ was removed via vigorous treatment with ethanol to remove impurities present along with it. The resultant solid residue was brown in colour and it was dried under vacuum at 55 °C to get powdered GO.

2.3. Preparation of the rGO-FSWCNT composite

FSWCNT were obtained from the laboratory itself as pristine Single-walled Carbon Nanotube were covalently functionalized for our previous research work as reported earlier [14]. Briefly, 3 gm of prepared GO powders were dispersed in 150 mL of ethanol under ultrasonic treatment for 3 h, followed by 6 g of FSWCNT and 0.6 g of hydrazine hydrate. The addition of hydrazine hydrate acts as a reducing agent that can induce the reduction of –COOH, epoxide ring and therefore exhibited interionic attraction to D-tryptophan attached to FSWCNT as shown in Fig. 1. The mixture was stirred for 14 h at 25 °C, and then washed with deionized water via a number of centrifugation cycles.

2.4. Fabrication of membrane by IP process

The IP process was used to prepare the nanocomposite membrane, where TMC was used as a cross-linker to fabricate the suitable reactive amide bond for enantioseparation. Fig. 2 represents the reaction scheme of IP process as shown below. According to our previously reported work, pure polysulfone (PSf) membranes were prepared to facilitate the IP process over its surface [15]. The fabrication of chiral polyamide layer over composite membranes was carried out through IP [20]. First, PSf sheets were soaked into the organic phase (25 mL, 0.5 % w/v TMC/ n-hexane) for 10 min at 25 °C. Afterward, excess of the solution was drained off from membrane surface under atmosphere, followed by its aqueous treatment solution of rGO-FSWCNT at the various composition of (1%, 3% and 5%), w/v for 5 min. Afterward, the membranes were cured at a temperature of 50 °C for almost 20 min. Finally, the membranes were thoroughly rinsed with deionized water and then the

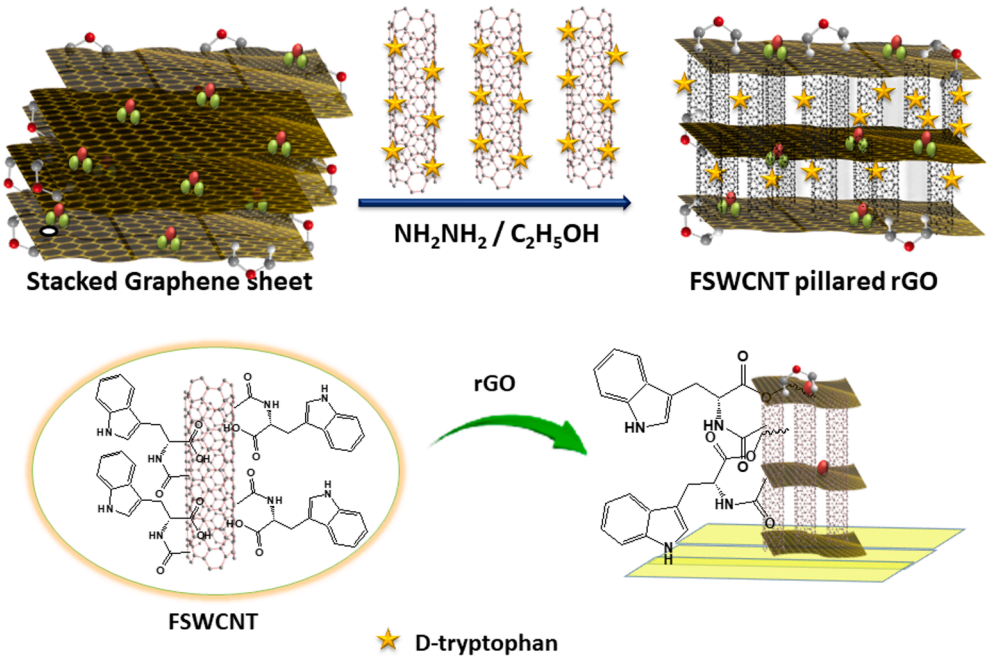

Fig. 1. Schematic Representation of formation of rGO-FSWCNT composite.

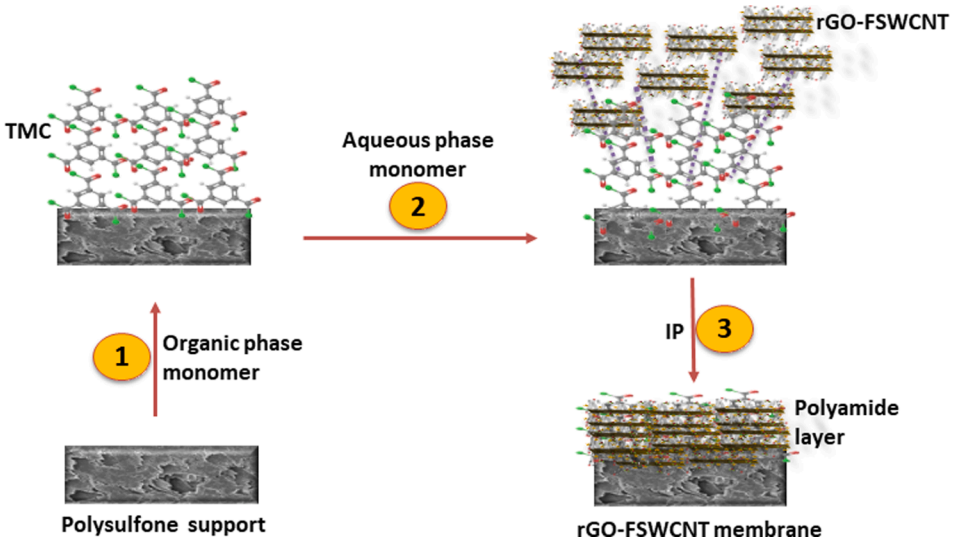

Fig. 2. Reaction scheme of IP of rGO-FSWCNT membrane.

residual part of TMC was removed at room temperature for use. The obtained membranes were denoted as M_{GC1}, M_{GC2} and M_{GC3} and the details of each composition are given in Table S1 of the supplementary material.

2.5. Characterization of the GO, rGO-FSWCNT composite and membranes

The functional group determination of GO, rGO-FSWCNT composite, M_{GC1}, M_{GC2} and M_{GC3} membranes were carried out by Fourier Transform Infrared (FTIR) analysis, Perkin Elmer, 2000 spectrophotometer. X-ray diffraction of GO and rGO-FSWCNT composite were studied using Bruker D-205505 Cu-kα radiation (λ = 1.5406 Å). Morphology of M_{GC1}, M_{GC2} and M_{GC3} was analyzed by Atomic Force Microscopy (AFM), using (WITec Atomic Force Microscope alpha 300 A). Field Emission Scanning Electron Microscopy further characterized the surface overview of GO, rGO-FSWCNT composite and cross-sectional membrane morphology at an electrical potential of 3 kV (FESEM, LEO 1427 VP, UK). X-ray photoelectron spectroscopy was used to determine the percentage of elements and their binding energy shift in the case of GO, rGO-FSWCNT composite, M_{GC1}, M_{GC2} and M_{GC3} membranes. This analysis was conducted in monochromatic radiation of Al Kα at a potential of 1486.6 eV. Sur PASS^{TM} Electrokinetic Analyzer was used to determine the streaming potential and surface charge acquisition of M_{GC1}, M_{GC2} and M_{GC3} membranes. The determination of thermal stability of composite membranes was determined using PERKIN Elmer PC series, DSC 7. The contact angle measurement of water on the M_{GC1}, M_{GC2} and M_{GC3} membranes was measured by a standard contact angle analyzer (DM-501, Kyonea Interface Science) at room temperature. Condensation Capillary Flow Porometer (Porous Materials, Inc., Model no. CCFP-5A) was used to determine the pore size distribution of the developed nanocomposite membranes

2.6. Separation study

Membrane-based separation of chiral isomer was carried out in a series of three number of two-compartment membrane cells. The flow diagram of membrane permeation setup for chiral separation of a racemic mixture is given in our previous publication [14,15]. Initially, three separate permeation experiments were run using prepared membranes (M_{GC1}, M_{GC2} and M_{GC3}). The different membrane setup was used in the permeation experiment for separation of DL-Tyrosine mixture under standard permselective parameters- pressure of 4 bar, feed concentration of 10 mmol.L^{-1}, a constant flow rate of 25 mL.min^{-1} and temperature of 35 °C, which is in accordance with our previously reported data [14]. After examining the performance of all membranes, relatively, the better-performed membrane was considered for the separation study of other four amino acids- DOPA, 1-methyltryptophan, tryptophan and threonine.

Three pieces of membrane (area 20 cm^2) were fitted into three different two-compartment cells during the permeation setup. The feed was circulated through an upper inlet of the membrane applying pressure in a continuous process [21]. The water permeate was collected at the lower outlet of the membrane cell at a time interval of 1 h and the permeates were analyzed using UHPLC model Dionex (Thermo Fisher Co.). The UHPLC analysis was conducted using a chiral column, CHIROBIOTIC ® T (column diameter 25 cm × 4.6 mm, 5 µm). The sample was injected into the column. The maxima of absorption for each racemic mixture were detected at a definite wavelength, as mentioned in Table S2. The chromatogram of UHPLC showed the particular peak area for each of the isomers, which was compared with standard calibration curves to resolute the concentration of an enantiomer in a racemic mixture. The quantification of a particular isomer present in the permeate solution was calculated using an equation of enantiomeric excess [15].

3. Results and discussion

3.1. Characterization of GO and rGO-FSWCNT composite

The characterization of GO and rGO-FSWCNT composite were done by Fourier Transform Infrared analysis (Figure S1), X-ray Photoelectron Spectroscopy and Field Emission Scanning Electron Microscopy. The result of FTIR analysis is briefly discussed in the supplementary material. Hydrazine hydrate was used as a reducing agent for the in-situ reduction of graphene oxide. The reduced groups of GO sheets become sufficiently reactive. Therefore, on the addition of FSWCNT, a type of pillaring effect is observed within the nanosheets. This effect becomes more prominent with an increase in interlayer distance. This pillaring nature of CNT can prevent the restacking ability of layered graphene sheets [22].

Synthesized GO and rGO-FSWCNT composite were scanned at a nanoscale level to obtain their XPS spectra. The oxygen to carbon proportions percentage ratio in synthesized GO was 32.31 % and 67.69 %, respectively. XPS wide scan spectra of rGO-FSWCNT show a significant decrease in the proportion of carbon to oxygen (32.31 to 8.17 %) due to an increase in carbon content from FSWCNT and a reduction in oxygen content at the surface. High-resolution peak fitting spectra for C1s were done in origin software. The results are shown in Fig. 3. The deconvulated C1s peak mainly contributed to C═C, hydrocarbon (C—C), hydroxyl (COX), C═O/O—C—O and carboxylic functionality peaks. Thus, the C1s XPS spectra of GO were fitted with different carbon environments such as hydrocarbon (C═C) at 284 eV, (C—C/C—H) at 285.2 eV, (C—O) at 286 eV, (C—O—C) at 287 eV and (C═O/O—C—O) at 288 eV whereas C1s XPS spectra of the rGO-FSWCNT composite were fitted with a number of carbon environments, correspond to (C—C/C—H) at 284.7 eV, (C—N) at 285.2 eV, (C—O) at 286.7 eV and (C═O/O—C—O) at 288 eV [20,21].

The morphological differentiation between bare GO, FSWCNT and rGO-FSWCNT composite membranes were carried out by FESEM investigation and are presented in Fig. 4. In Fig. 4(a), the surface morphology of GO evinces wrinkled and stacked silk-lined nanosheets.

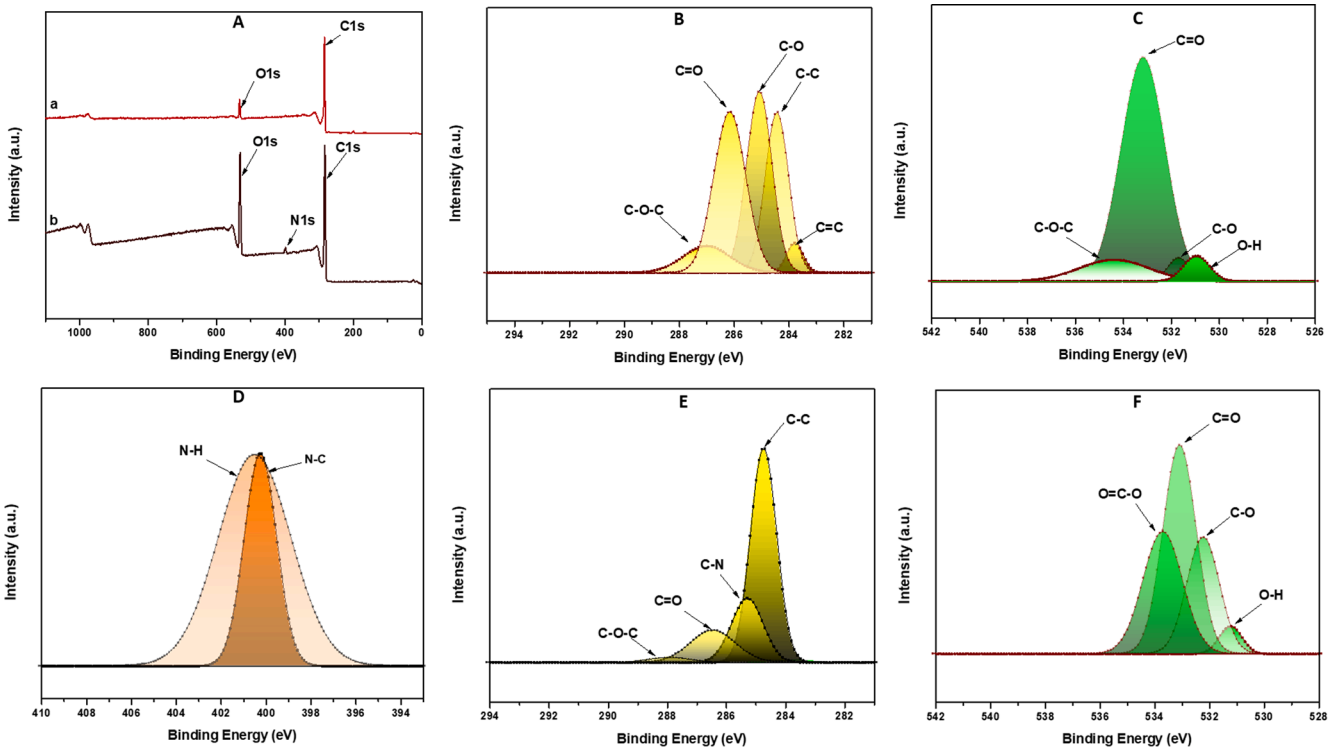

Fig. 3. XPS spectra of (A) GO (B) rGO-FSWCNT composite.

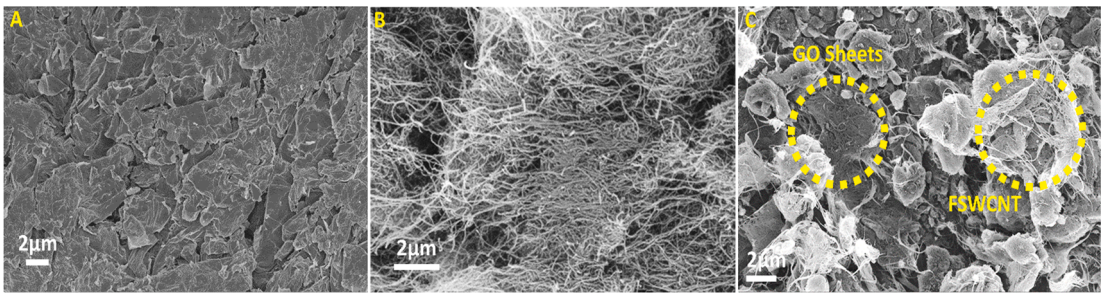

Fig. 4. FESEM image of (A) GO (B) FSWCNT (C) rGO-FSWCNT composite.

Fig. 4(b) represents a Fibrous organisation of FSWCNT and Fig. 4(c) represents the hybrid rGO-FSWCNT systems which comprises interconnected assembly of both GO nano-sheets and as well as FSWCNT fibers. In the rGO-FSWCNT composite system, the FSWCNT moieties get intercalated between the adjacent GO sheets, leading to the expansion of the inter laminar galleries. This interconnected network of expanded nanochannels provided a rather smooth pathway for the desired isomer to pass through and hence enhanced the performance hybrid rGO-FSWCNT membrane towards the desired compounds [21–22]. The successful intercalation of the FSWCNT moieties into the inter laminar galleries of adjacent GO sheets was verified from PXRD pattern analysis which is shown in Fig. S2. Bare GO shows characteristics XRD reflections corresponding to the plane (0 0 1) at 2θ of 11.9° (Figure S2 (a)) and the interlayer spacing corresponding to this peak was calculated as 0.74 nm. Intercalation of FSWCNT into the GO laminar galleries expanded the distance between the neighboured graphene sheets and accordingly the interlayer spacing shifted to 1.43 nm for the hybrid rGO-FSWCNT composite as shown in Figure S2 (b).

3.2. Characterization of membranes

After modifying rGO-FSWCNT membranes (M_{GC1}, M_{GC2} and M_{GC3}), different functional groups' change in molecular vibration was elucidated by the Fourier transformed infrared (FTIR) spectroscopy in Fig. 5. In Fig. 5 (a), (b) and (c), the characteristic peaks at 1254, 1359, 1285, and 1559 cm^{-1} attribute to symmetric stretching of C—O—C, O═S═O, S—O and C—C, respectively [21,23]. These are observed for raw PSf. The polymerization reaction at the interface of amine and acid chloride represents the characteristics peak of amide at 1600–1654 cm^{-1}. Therefore, the two most prominent vibrations of C═O and N—H were observed at 1652 and 1610 $cm^{-1,}$ as shown in Fig. 5 (b). Moreover, the absorption peak at 1546 – 1762 cm^{-1}correspond to the presence of C═C and C═O of D-tryptophan. Furthermore, the bands at 1223 cm^{-1} and 848 cm^{-1} confirm epoxy groups that comply with symmetric and deformation vibrations, respectively [23].

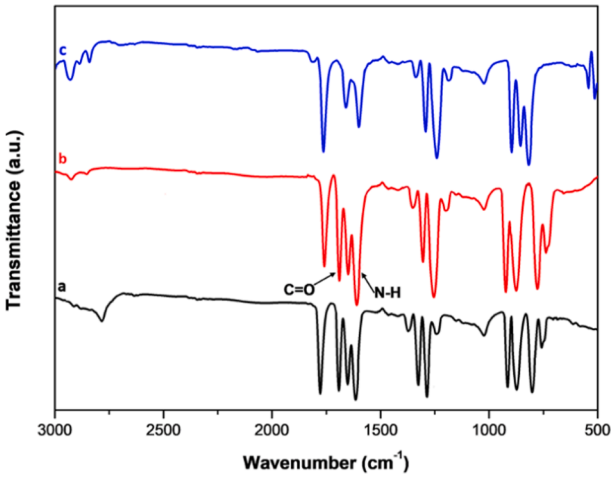

Fig. 5. FTIR spectra of (a) M_{GC1} (b) M_{GC2} and (c) M_{GC3}.

X-ray Photoelectron Spectroscopy (XPS) is one of the standard characterization techniques that can use an electron beam to penetrate through 5 nm of the inside membrane surface. The binding energy shift of different chemical compositions present in M_{GC1}, M_{GC2} and M_{GC3} membranes were determined as shown in Fig. 6. In general, this characterization technique was used to evaluate the percentage composition of elements present in the polymeric surface. The wide scan XPS survey of M_{GC1}, M_{GC2} and M_{GC3} membranes are shown in Fig. 6 (A), which depicts the presence of carbon (C1s), oxygen (O1s), nitrogen (N1s) and sulphur (S2p) for all the membranes. Moreover, Fig. 6 (C.1, D.1 and E.1) represents the high-resolution scan of N1s, and it results in two peaks at a binding energy shift of 398.7 and 400.1 eV, respectively, which determines the presence of N-H and N-C═O in the cross-linked polymeric structure [15].

High-resolution C1s scan of M_{GC1}, M_{GC2} and M_{GC3} membranes are shown in Fig. 6 (C.2, D.2 and E.2), which represents the binding energy shifts at 284.3, 284.6, 284.7, 286.7, 285.5, 288 and 288.9 eV respectively, which is in accordance with C—S, C═C, C—C, C—O, C—N, C═O and N—C═O/O—C═O respectively [14]. The high-resolution scan of C1s showed a difference in chemical composition between M_{GC1}, M_{GC2} and M_{GC3} membranes.

The high-resolution O1s scan of M_{GC1}, M_{GC2} and M_{GC3} membranes are shown in Fig. 6 (C.3, D.3 and E.3) within the range of 530–536 eV. The binding energy shift of the carbonyl group at 532 eV signified the formation of an amide bond. S═O represents binding energy shift at 532 eV with an intense peak of C—O at a binding value of 533.8 eV [20]. The wide scan XPS spectra of the S atom signifies the presence of C—S and O═S═O bond at 167.6 and 168.1 eV, respectively, as shown in Fig. 6 (C.4, D.4 and E.4).

The potential applications of prepared membranes are determined by thermogravimetric treatment. Therefore, the membranes were treated under an elevated nitrogen atmosphere with a heat flow rate of 10 °C.min^{-1}. In Fig. 7 (b), the first step of decomposition determines the temperature of desorption of water molecules and is observed at a temperature region of 80–110 °C with weight loss of 4.5 wt%, followed by significant decomposition at temperatures of 484, 514, 518 and 521 °C for PSf, M_{GC1}, M_{GC2} and M_{GC3} membranes respectively. The higher degradation temperature of M_{GC3}can be illustrated with the effective interaction of CNT and reduced GO through pillared configuration. This pillaring effect of rGO-FSWCNT contributed to the head-on overlapping of FSWCNT vertically to the edge of rGO sheets. This can be ascribed from the more vital interaction of the amide group adjacent to the edges of FSWCNT and the reduced functional group present in GO sheets [15,21].

Fig. 8(A.1, A.2 and A.3) represents the surface morphology and (B.1, B.2 and B.3) depicts the cross-sectional image of M_{GC1}, M_{GC2} and M_{GC3} membranes. On continuous polymerization, two monomer solutions showed significant influence on morphology. The morphological view of three developed membranes indicates that the surface is relatively

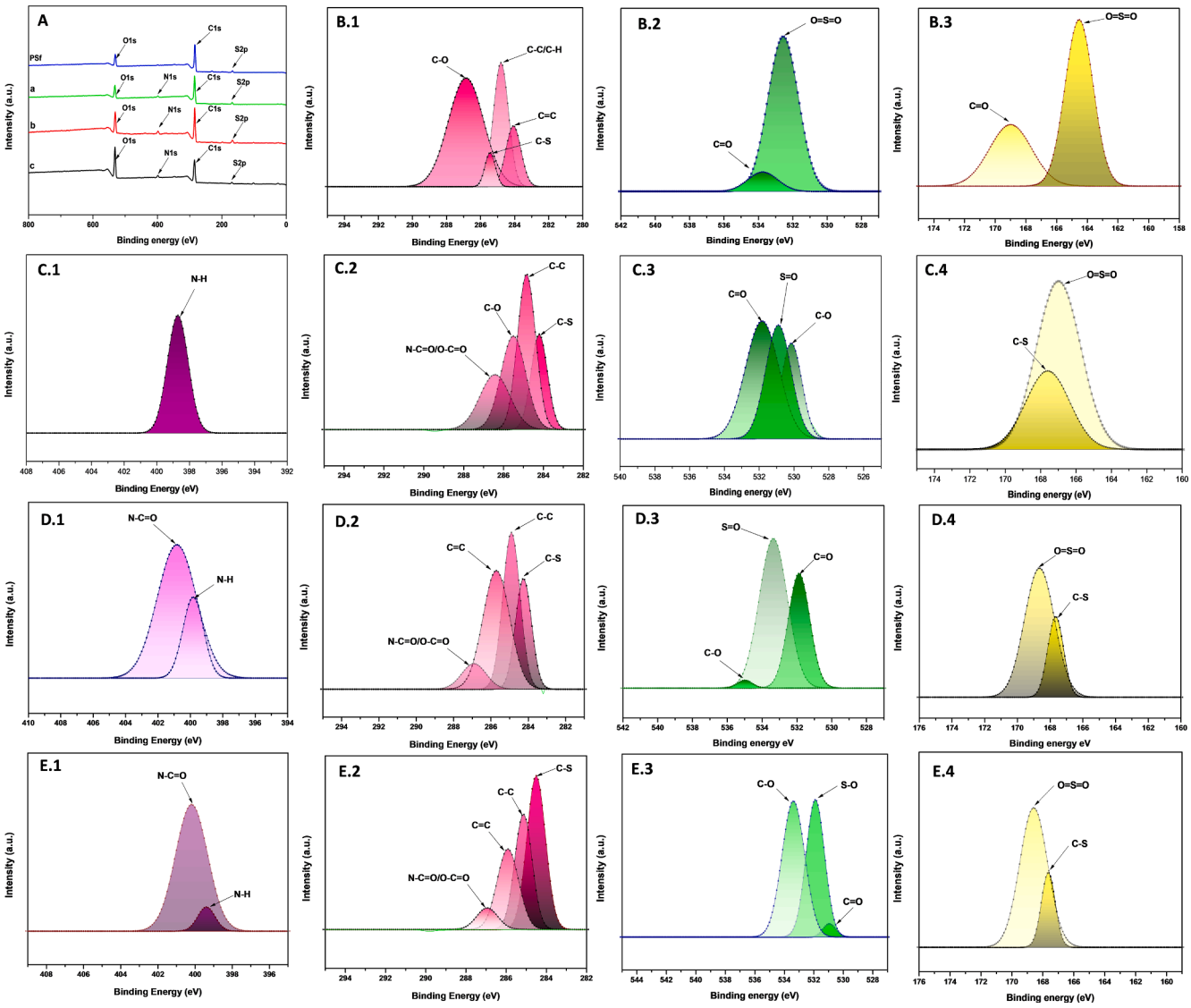

Fig. 6. XPS spectra (A) Survey scan; (B.1, B.2 and B.3) C1s, O1s, S2p wide scan of PSf membrane; (C.1, C.2, C.3 and C.4) N1s, C1s, O1s and S2p wide scan of M_{GC1}; (D.1, D.2, D.3 and D.4) N1s, C1s, O1s and S2p wide scan of M_{GC2} and (E.1, E.2, E.3 and E.4) N1s, C1s, O1s and S2p wide scan of M_{GC3}.

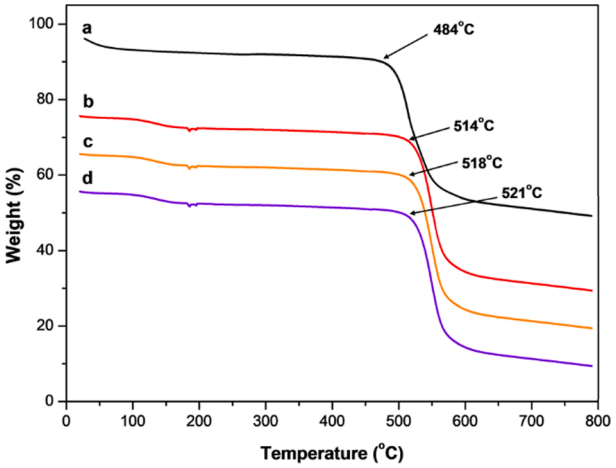

Fig. 7. TGA spectra of (a) PSf (b) M_{GC1} (c) M_{GC2} and (d) M_{GC3}.

smooth with some nanoscale ripples. The cross-sectional images revealed that the membrane showed well-defined asymmetric projections, covered with a dense layer on an upper surface with a macrovoid's distribution in their sublayer portion. Those projections of membrane pores are typically interconnected with their macro-voids [21]. As seen in the cross-section view of the three different nanocomposite membranes it seems like the thickness of the membrane surface slightly increases on loading the amount of rGO-FSWCNT from 1% to 3%. These morphological changes are due to the addition of rGO-FSWCNT during interfacial polymerization, the functional groups on the surface of rGO-FSWCNT could interfere with the hydrogen bonding dynamics while making the thin selective polyamide layer. Increasing the concentration of rGO-FSWCNT from 3% to 5% lead to the agglomeration on the membrane surface. This resulted in membrane pore blocking, eventually leading to rheological hindrance in the interaction between the chiral probe and the enantiomers. This can be clearly seen from the surface image of M_{GC3} membrane as shown in Fig. 8(A.3). Therefore, the chiral membrane surface was explicitly designed to obtain the highest percentage of enantiomeric excess for racemic mixtures.

Atomic Force Microscopic technique was used to determine the topographic view of M_{GC1}, M_{GC2} and M_{GC3} membrane. Lamellar

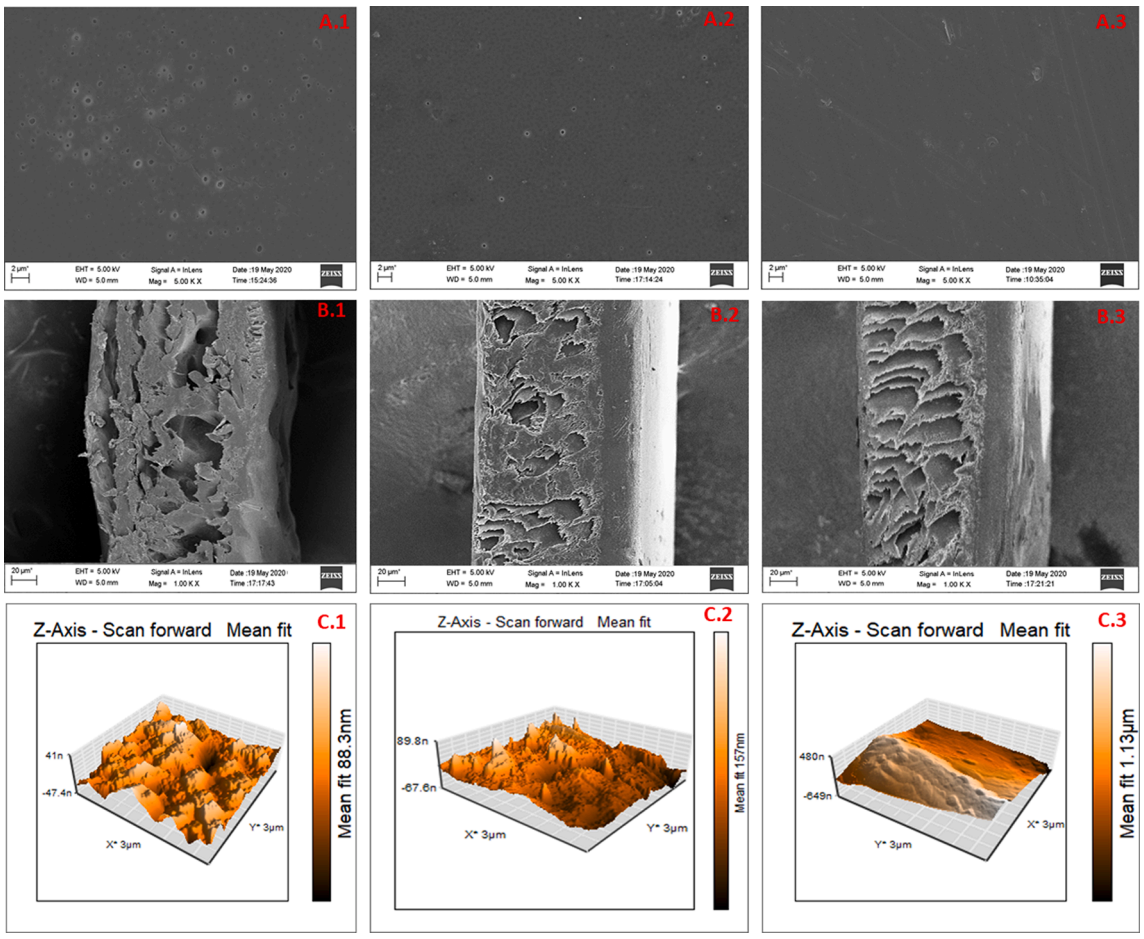

Fig. 8. FESEM image (A.1, A.2, A.3) Surface Morphology (B.1, B.2, B.3) Cross-sectional view; (C.1, C.2, C.3) AFM images of M_{GC1}, M_{GC2} and M_{GC3} membrane.

orientation of membrane surface is shown here, where the outer surface roughness of membranes was scanned within the area of 3 × 3 µm in Fig. 8 (C.1, C.2 and C.3). Therefore, the scanning area of membrane surface showed nodular valley-like morphology of modified membrane, which was indicated by respective bright and dark regions. The outer surface area seems very rough. The nodules are distributed in a fused manner with each other, which possesses the stronger intermolecular attraction between rGO-FSWCNT and the polymeric support [20,21]. Since there is a strong hydrogen bonding due to the interaction of hydroxyl groups of the rGO-FSWCNT, the agglomeration rate diminishes and portrays uniform dispersion of rGO-FSWCNT in case of M_{GC2} membrane. After enhancing the concentration of rGO-FSWCNT up to a certain level from 1% to 3%, the membrane surface roughness increased. Further, there occurs surface deformation upon increasing the concentration of rGO-FSWCNT from 3% to 5% which might be due to the agglomeration of higher concentration of rGO-FSWCNT as depicted in Fig. 8(C.3).

A standard sessile drop method was used to determine the hydrophilicity of prepared M_{PSf}, M_{GC1}, M_{GC2} and M_{GC3} membranes. It can be stated that the interface energy of water drop is related to the properties of the polymeric matrix. Therefore, we have determined the contact angle and surface interfacial energy for each of the prepared

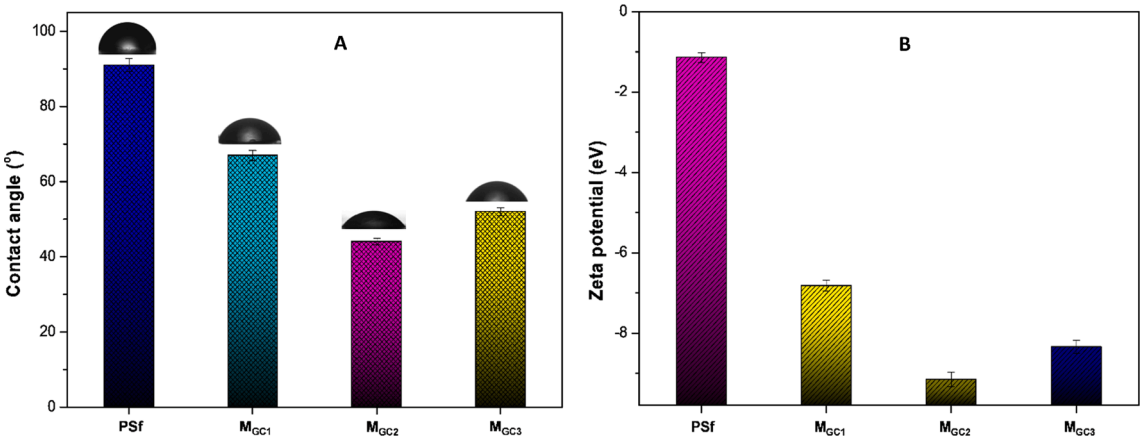

Fig. 9. (A) Contact angle; (B) Zeta Potential of the PSf, M_{GC1}, M_{GC2} and M_{GC3} membranes.

membranes. In Fig. 9(A), an arrowhead was used to determine the angle between liquid drop with its contact membrane surface. The contact angle of the raw PSf membrane is found to be (91 ± 1.82)° and determines the membrane surface wettability as hydrophobic. In the case of raw polysulfone membrane, the interface surface energy is relatively low when a drop of water comes into contact with its surface. Moreover, the prepared rGO/FSWCNT based composite membrane possesses many polar groups that exhibit hydrogen bonding affinity with the inward pulling of water molecules. Therefore, their interface surface energy will be higher with a strong affinity of non-bonding adhesive forces [15,21]. Their higher surface energy value is strongly driven by the adequate hydrogen bonding of –CONH– with a hydroxyl group of water molecules. This strongly evidences the hydrophilic nature of the membrane surface in a well-defined CNT pillar within the reduced GO sheets over PSf support. In view of this, M_{GC1} showed a contact angle at about (67 ± 1.34)° as seen in Fig. 9(A). A dynamic water contact angle of (44 ± 0.88)° was observed in the case of M_{GC2}, due to which it possesses a higher degree of adhesive forces towards water molecules with adequate intermolecular hydrogen bonding. As a result of which, the membrane possesses highest interface energy of 87.24 $mJ.m^{-2}$. With an increase in the concentration of rGO-FSWCNT in the case of M_{GC3}, the accumulation of their bulkier pillared fragment over PSf support causes a drastic decrement in interface energy with an increase in water contact angle to (52 ± 1.04)°. Moreover, the appearance of a nodular cross-section at the membrane surface act as a suitable channel to carry the water molecules through adsorption within their pores [20].

Zeta potential analyzer was used to determine the streaming current and streaming potential of raw PSf, M_{GC1}, M_{GC2} and M_{GC3} membranes. Quantitative estimation of electrochemical potential was done by using 1 mM KCl solution at pH 7 at room temperature. Fig. 9(B) represents the zeta potential values of all prepared membranes. The process was initiated by dipping membranes on electrolyte solution for 30 min. Where, raw PSf membrane shows negative ζ-potential of − 1.14 mV, M_{GC1}, M_{GC2} and M_{GC3} membrane shows a surface potential at − 6.82, − 9.15 and − 8.34 mV, respectively. The observed value concluded that the amide bond facilitated the more significant negative potential in the rGO-FSWCNT based membrane than the raw PSf. The negative zeta potential observed in the different rGO-FSWCNT hybrid systems can be attributed to the oxygen-functionality present in the amide bond. So, we expect zeta potential values to increase gradually with the increase in mass loading of rGO-FSWCNT. Accordingly, the membrane's negative zeta potential value increases with the increase in mass loading of rGO-FSWCNT from 1% to 3%. The observed slight retardation of negative zeta potential of the membrane with further increase in the mass loading of 5% of rGO-FSWCNT may be due to the self-agglomeration of the surface exposed reactive functional group via hydrogen bonding formation between –CONH- bonds. The corresponding contact angle measurement shows the same trend where membrane hydrophilicity increases from PSf to M_{GC2} due to increased surface-exposed hydrophilic –CONH- functional groups. But again, for M_{GC3} membrane, the contact angle value was observed to be greater than M_{GC2} membrane. This also gives us a brief hint about self-association of the hydrophilic surface-exposed –CONH- functional groups due to which membrane hydrophobicity increases on going from M_{GC2} to M_{GC3} membrane [15,21].

3.3. Chiral separation

The quantitative effect of different physicochemical parameters on chiral separation process using the prepared membranes is described here. Separation experiments were conducted using M_{PSf}, M_{GC1}, M_{GC2} and M_{GC3} membranes containing 0%, 1%, 3% and 5% rGO-FSWCNT as the aqueous monomer. Two-compartment membrane fitted cells were used separately to separate DL-Tyrosine under selective parameters-pressure of 4 bar, feed concentration of 10 $mmol.L^{-1}$ and flow rate of 25 $mL.min^{-1}$ at 25 °C [14]. Moreover, the effect of the concentration of rGO/FSWCNT on flux and enantiomeric excess (% ee) for racemic tyrosine was studied. Fig. 10 (A) shows the variation of membrane flux for L- and D-isomer after 8 h for each membrane separately. The obtained results have evaluated the highest difference in membrane flux in the M_{GC2} membrane containing 3% of rGO-FSWCNT, corresponding to 39.56 and 0.19 $mmol.m^{-2}.h^{-1}$ for L- and D- isomer of tyrosine, respectively. The higher membrane flux for L-tyrosine may be due to the selective adsorption of its D-isomer into the nanocomposite membrane, followed by its self-association behavior with chiral probe [15]. Fig. 10 (B) represents the variation of $ee_{L\text{-tyrosine}}$ (%) after conducting 8 h of membrane for four different membranes, respectively, where the highest ee of M_{GC2} was obtained as 96%. The highest $ee_{L\text{-tyrosine}}$ (%) of ~ 99 % was recorded for M_{GC2} membrane. The quantitative effect of M_{GC2} membrane on different flux values could be explained in terms of the contact area between the D-isomer and the chiral probe present. With an increase in the contact area of D-isomer, the rate of its mass transfer into the membrane surface was increased; therefore, the D-isomer of tyrosine was bonded stereospecifically with a chiral probe introduces into the membrane, where its antipode was retentate by membrane pores [14]. Eventually, the gradual decrease of $ee_{L\text{-tyrosine}}$ (%) is also observed with increasing rGO-FSWCNT to 5%. Therefore, M_{GC2} membrane was selected for the detailed separation of the other four β-substituted-α-amino acids–1-methyltryptophan, DOPA, tryptophan and threonine.

The effect of permeation time on the separation behavior of DL-tyrosine is shown in Fig. 11 (A.1 and B.1). The membrane flux of L-isomer tends to decreases from 74.32 to 38.13 $mmol.m^{-2}.h^{-1}$ within a time duration of 1 h to 10 h, whereas, for D-isomer, the flux value was changed from 21.52 to 0.71 $mmol.m^{-2}.h^{-1}$. Gradually, it can be observed that the flux value reaches a point of saturation after 8 h of

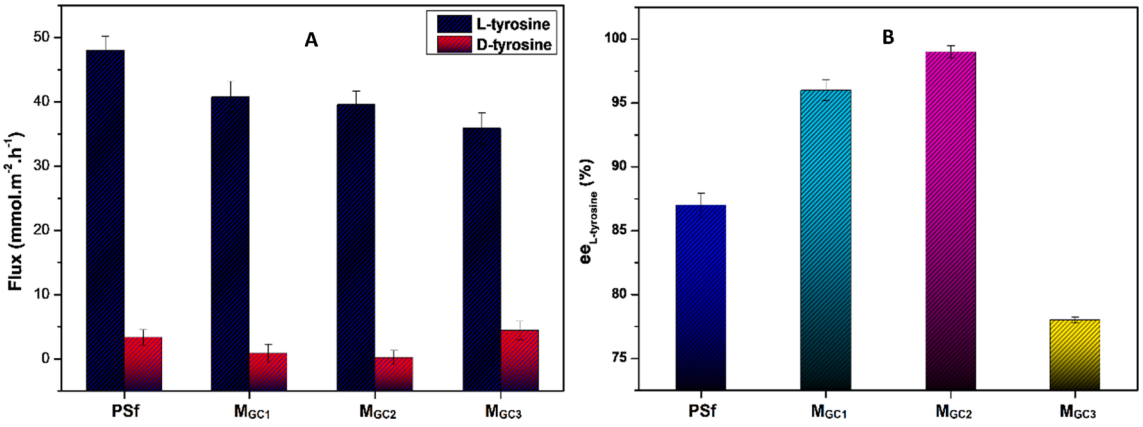

Fig. 10. Effect of concentration of rGO-FSWCNT on the flux and $ee_{L\text{-tyrosine}}$ (%), where operating pressure of 4 bar, feed concentration of 10 $mmol.L^{-1}$, a constant flow rate of 25 $mL.min^{-1}$and temperature of 25 °C.

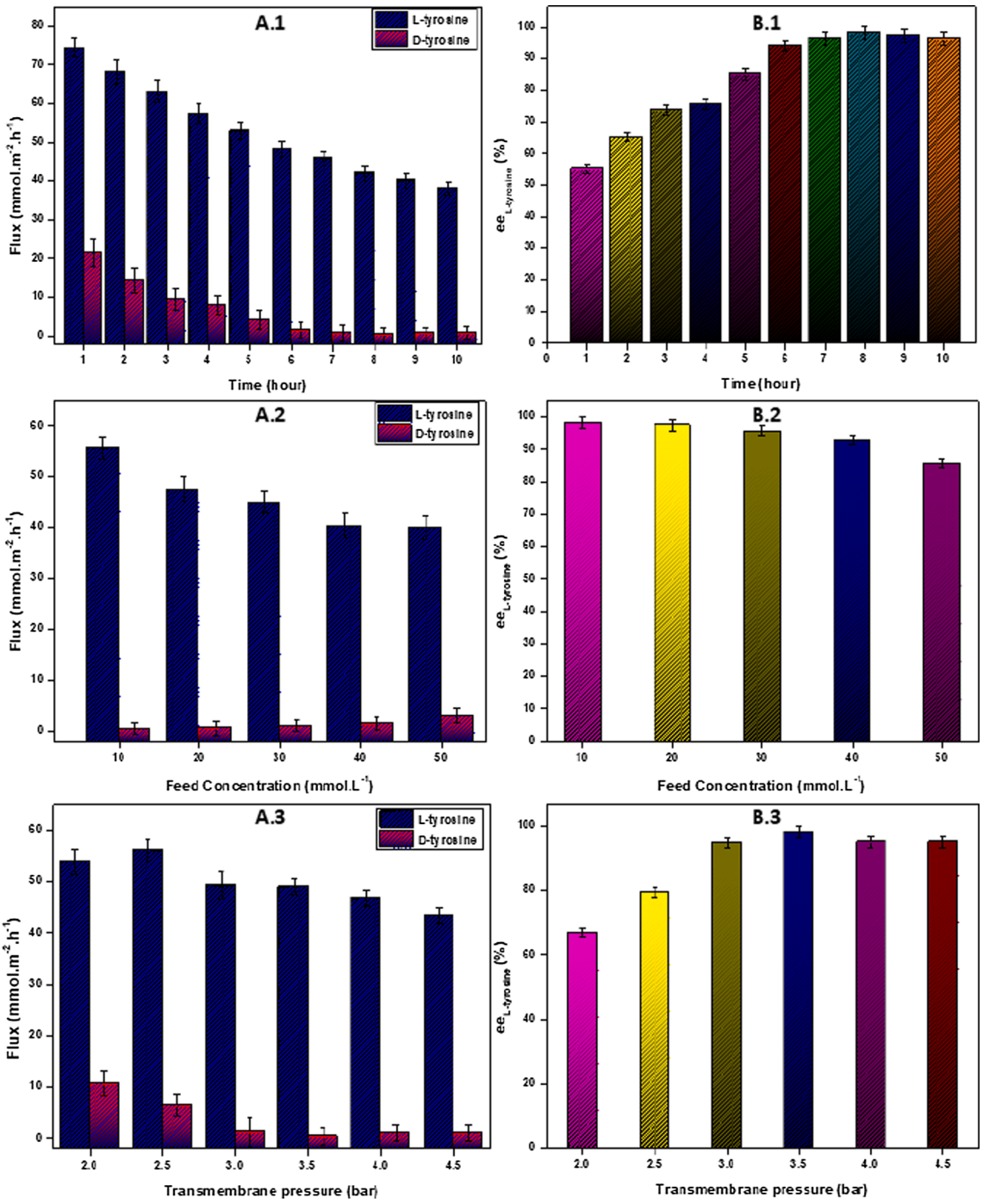

Fig. 11. Effect on DL-tyrosine upon membrane treatment in terms of (A) flux (B) $ee_{L\text{-tyrosine}}$ (%) values (A.1 and B.1) Change in permeation time; (A.2 and B.2) Change in feed concentration; (A.3 and B.3) Change in operating pressure at a constant flow rate of 25 mL.min^{-1}and temperature of 25 °C.

membrane-based treatment of racemic tyrosine. Similarly, the increase in enantiomeric excess of L-tyrosine is also observed from 55.08 to 98.3 % during the time of membrane permeation. Further, the rise in permeation time upto 10 h, the significant change of $ee_{L\text{-tyrosine}}$ (%) is not observed. This consistency can be obtained in accordance with the saturation of chiral moiety over the membrane surface [15].

Another factor, such as feed solution concentration, also contributed to observable change in the separation behavior for DL-tyrosine during membrane permeation. At an initial concentration of 10 mmol.L^{-1}, the maximum $ee_{L\text{-tyrosine}}$ (%) was observed as 98.3 %. Further, the saturation behavior of chiral moiety was increased with increasing the feed; therefore, the membrane flux for L-tyrosine decreases from 55.67 to 38.65 mmol.m^{-2}.h^{-1}, where D-tyrosine starts to adsorb within the membrane and the trend of flux value was observed from 0.47 to 5.29 mmol.m^{-2}.h^{-1}. The significant decrease of $ee_{L\text{-tyrosine}}$ (%) value was obtained as 85.67 %, with further increase in feed concentration up to 50 mmol.L^{-1}. The transmembrane pressure is an essential thermodynamic parameter to determine membrane performance. Therefore, we have studied the pressure effect on membrane flux and $ee_{L\text{-tyrosine}}$ (%). For the first time, the membrane flux for both of the isomers of tyrosine sharply decreases. Their consistency was maintained upon further increase of membrane pressure, shown in Fig. 11(A.3 and B.3). The $ee_{L\text{-tyrosine}}$ (%) value was increased up to 98.3 % at a pressure of 3.5 bar and the decrement in the $ee_{L\text{-tyrosine}}$ (%) value was observed at 95.2 % due to

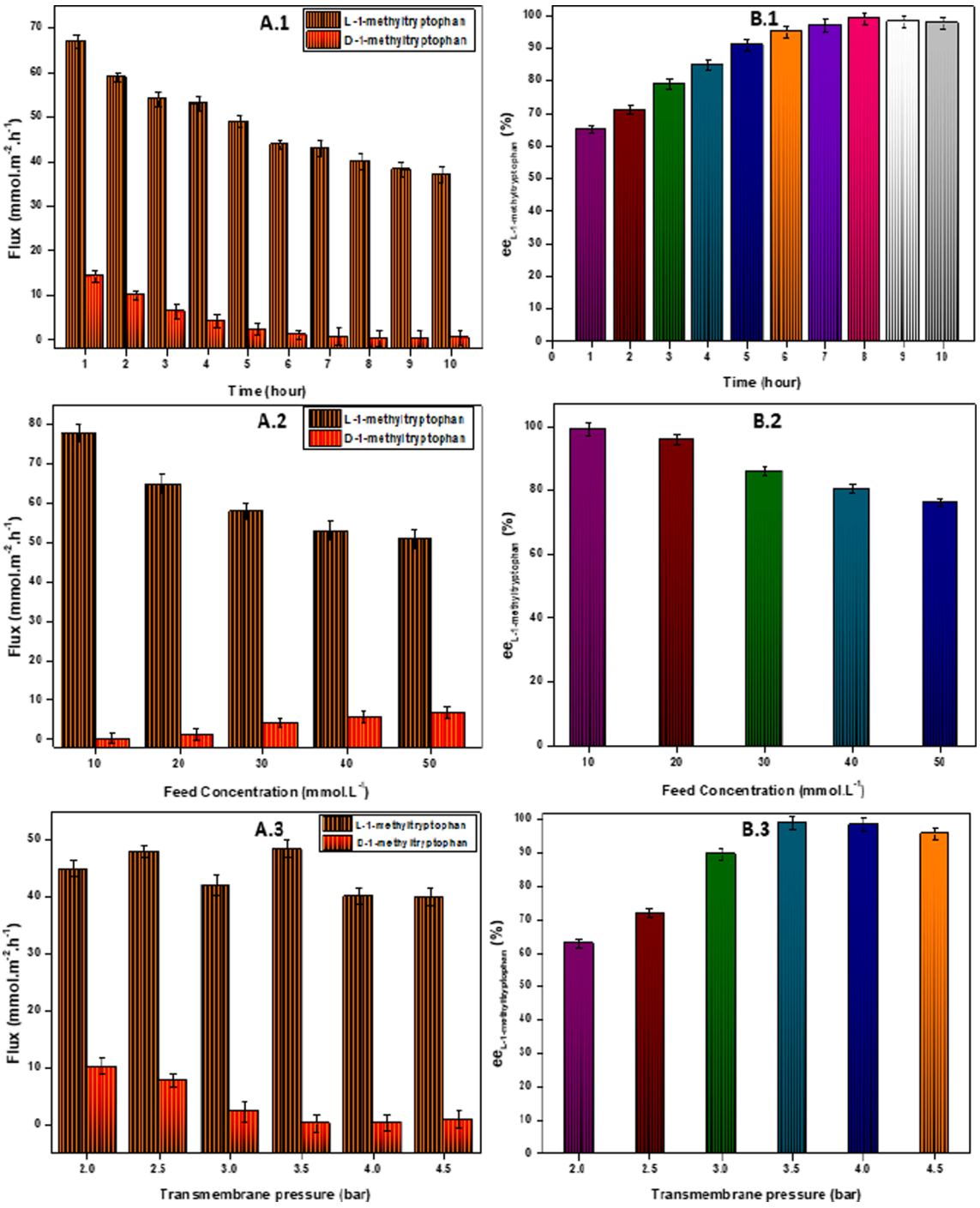

Fig. 12. Effect on DL-1-methyltryptophan upon membrane treatment in terms of (A) flux (B) $ee_{L\text{-}1\text{-}methyltryptophan}$ (%) values (A.1 and B.1) Change in permeation time; (A.2 and B.2) Change in feed concentration; (A.3 and B.3) Change in operating pressure at a constant flow rate of 25 mL.min^{-1} and temperature of 25 °C.

the permeation flux and membrane selectivity [14,15].

In Fig. 12(A.1 and B.1), the separation behavior for DL-1-methyltryptophan was discussed with respect to the impact of permeation time. The membrane flux tends to decrease from 67 to 37.03 mmol.m^{-2}.h^{-1} for L-isomer, whereas in case of D-isomer, flux value was changed from 14.21 to 0.43 mmol.m^{-2}.h^{-1} with a change in permeation time from 1 h to 10 h. After 8 h of membrane permeation, the membrane flux will achieve a point of saturation. Similarly, the enantiomeric excess of L-1-methyltryptophan is also increased upto 99.02 % with an increase in permeation period up to 8 h. Furthermore, there is no notable change in $ee_{L\text{-}1\text{-}methyltryptophan}$ (%) upon increasing the permeation time after 8 h. This consistent membrane flux and enantiomeric excess are obtained in accordance with the saturation of chiral moiety over membrane surface [15].

The concentration of feed solution was further studied during the separation of DL-1-methyltryptophan after 8 h of permeation time. At an initial feed concentration of 10 mmol.L^{-1}, the $ee_{L\text{-}1\text{-}methyltryptophan}$ (%) was found to be at a maximum of 98.2%. Furthermore, the chiral moiety becomes saturated with an increase in concentration. Therefore, the flux value for L-isomer gradually decreases from 78 to 51 mmol.m^{-2}.h^{-1}. With further increase in feed concentration up to 50 mmol.L^{-1}, a significant decrease of $ee_{L\text{-}1\text{-}methyltryptophan}$ (%) value was obtained as 76.09%. The *trans*-membrane pressure also played an important role in determining membrane performance. Therefore, the effect of pressure

on membrane flux and $ee_{L\text{-}1\text{-}methyltryptophan}$ (%) is also considerable. Initially, the membrane flux for both isomer of tyrosine decreased sharply and their consistent quantified flux value was observed upon further increase of membrane pressure, as shown in Fig. 12 (A.3 and B.3). The $ee_{L\text{-}1\text{-}methyltryptophan}$ (%) value increases up to 99.2 % at a pressure of 3.5 bar and the decrement in the $ee_{L\text{-}1\text{-}methyltryptophan}$ (%) value was obtained at 95.76 % due to specific membrane selectivity.

Afterward, we have studied the M_{GC2} membrane-based permeation behavior of DL-DOPA. In Fig. 13 (A.1 and B.1), we have shown the effect of running permeation time on the separation of racemic DOPA in the assistance of flux and $ee_{L\text{-}DOPA}$ (%) values. From this, we have seen that there is a gradual decrease in flux value from 58.9 to 42.57 mmol.m^{-2}.h^{-1} for L-isomer and 17.59 to 0.88 mmol.m^{-2}.h^{-1} for D-isomer with an increase in the permeation time. The concomitant escalation of $ee_{L\text{-}DOPA}$ (%) was observed with respect to the variation of time where permeation flux gradually declines initially till the saturation point, as shown in Fig. 13 (A.1, B.1). The inconsistent decrease in the permeation flux of the complementary isomer was also observed. The proper orientation of reactive functionality on D-isomer is one of the chiral recognitions through which the isomeric inclusion could be observed [15,24]. The structural opposition of the L-isomer favored its permeability through the porous membrane and resulting in a high $ee_{L\text{-}DOPA}$ (%) value of 98.9

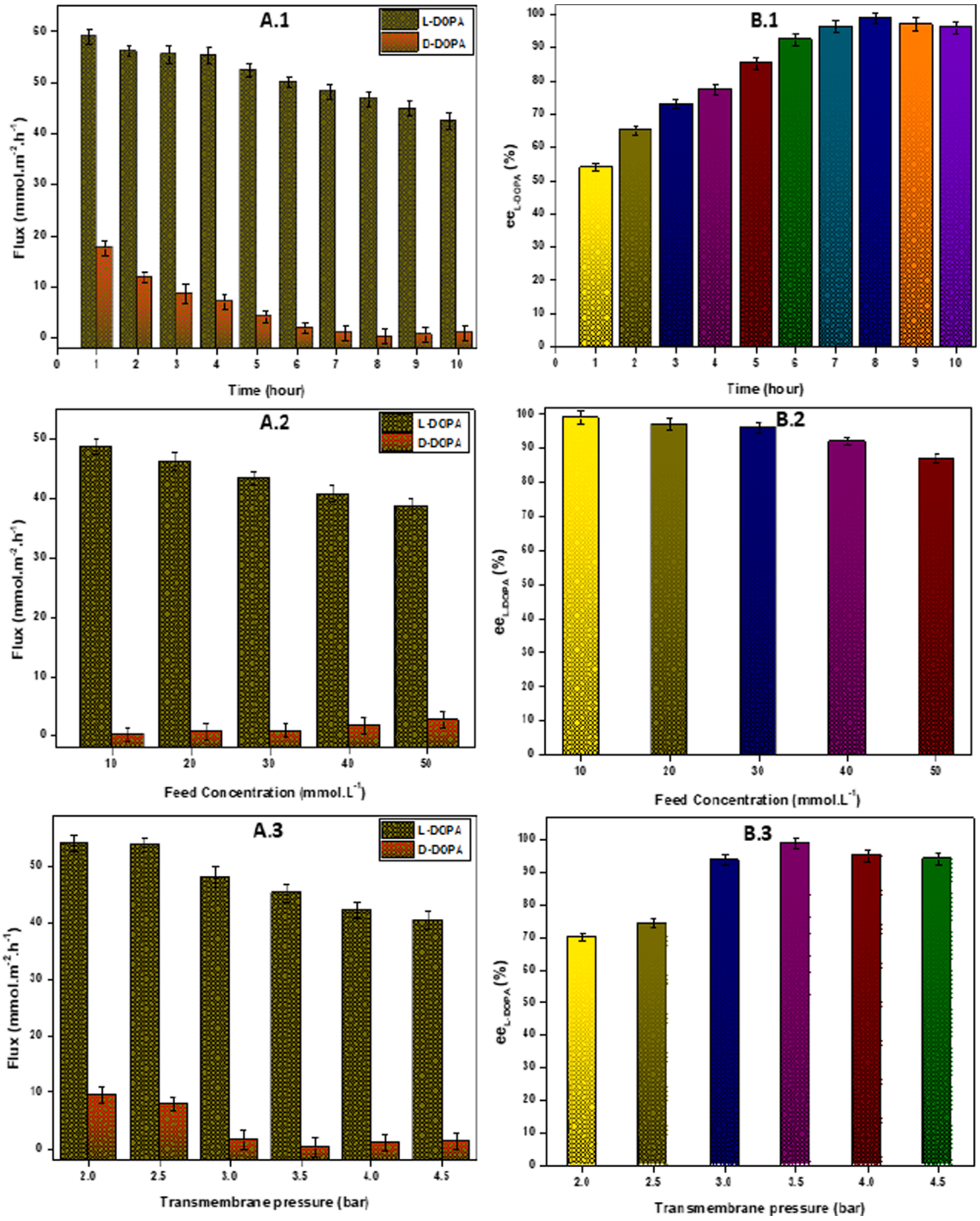

Fig. 13. Effect on DL-DOPA upon membrane treatment in terms of (A) flux (B) $ee_{L\text{-}DOPA}$(%) values (A.1 and B.1) Change in permeation time; (A.2 and B.2) Change in feed concentration; (A.3 and B.3) Change in operating pressure at a constant flow rate of 25 mL.min^{-1} and temperature of 25 °C.

%.

The concentration of feed solution is an effective parameter to study the membrane permeation behavior. Therefore, our work has focused on evaluating the effect of concentration on the enantiomeric excess and permeation flux of DL-DOPA. Fig. 13(A.2 and B.2) have determined that on increasing feed concentration from 10 up to 50 mmol.L^{-1}, the membrane flux gradually decreases. Moreover, the lower flux value was evaluated for D-DOPA due to its effective recognition with the chiral probe. The $ee_{L\text{-}DOPA}$ (%) values followed a downtrend from 98.9 to 87 % and its maxima were obtained at a feed concentration of 10 mmol.L^{-1}. This observation can be ascribed in terms of concentration polarization within the fibrous hybrid membrane. This process picturized that the membrane porosity gets perturbed due to the polarization of respective charged species, which is strongly dominated by steric crowding [25]. Henceforth, it could be explained that an increase in feed concentration suppressed the efficiency of chiral recognition of isomer towards membrane surface and delivered the rate of isomeric agglomeration over membrane surface and therefore, membrane flux gradually decreases.

Fig. 13(A.3 and B.3) represented the effect of *trans*-membrane pressure on the enantio-separation of DL-DOPA. With an increase in pressure from 2 to 4 bar, the membrane flux was decreased due to the increase in

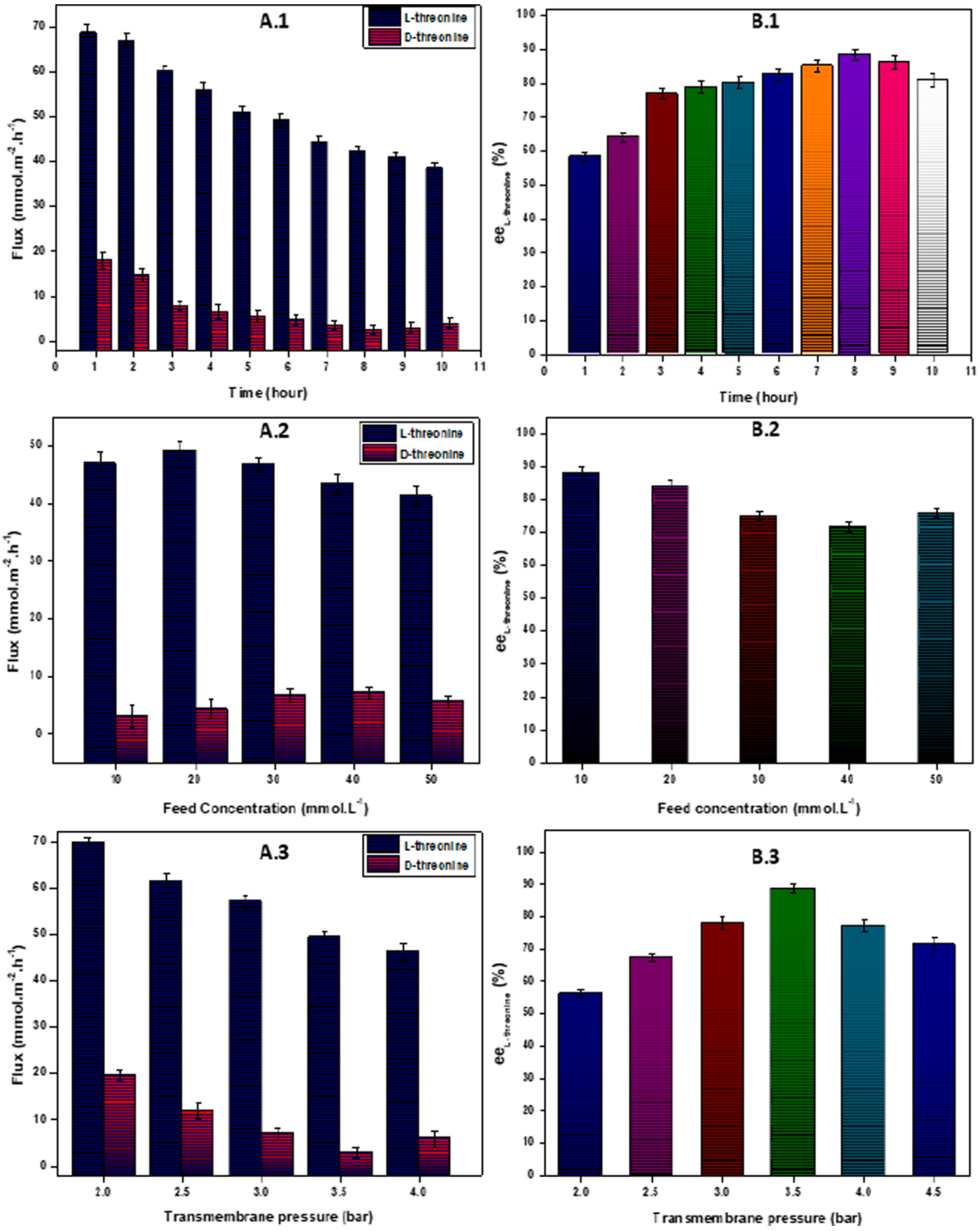

Fig. 14. Effect on DL-threonine upon membrane treatment in terms of (A) flux (B) $ee_{L\text{-threonine}}$ (%) values (A.1 and B.1) Change in permeation time; (A.2 and B.2) Change in feed concentration; (A.3 and B.3) Change in operating pressure at a constant flow rate of 25 mL.min^{-1} and temperature of 25 °C.

collision frequency between chiral probe and isomer, which can obstruct the rate of diffusion of isomer within the mixed-matrix membrane. The saturation of membrane pressure was also observed at 3.5 bar pressure, where D-isomer is involved with the more vital covalent interaction with chiral probe introduced into the nanocomposite membrane [15]. Further increase in pressure beyond 3.5 bar, the decrease in $ee_{L\text{-DOPA}}$ (%) value from 98.9 to 94.03 % was observed.

In Fig. 14(A.1 and B.1), the time-dependent membrane permeation for DL-threonine was observed to explain the deviation of membrane flux as well as enantiomeric excess. The change in membrane flux is inversely proportional to the time of membrane permeation, where the flux values tend to decrease from 68.83 to 38.56 mmol.m^{-2}.h^{-1} for L-threonine and 18.10 to 4.02 mmol.m^{-2}.h^{-1} for D-threonine during 1 h to 10 h. This can be observed that membrane flux value reached a point of saturation after 8 h of permeation. For 1 h of permeation, the $ee_{L\text{-threonine}}$ (%) value is about 58.34 % and it strongly increases to 88.45 %. Further, increasing the permeation time beyond 8 h, the $ee_{L\text{-threonine}}$ (%) value was obtained at 81.09 %. The consistency in $ee_{L\text{-threonine}}$ (%) value can be described by saturation of chiral moiety and more preferentially bound D-threonine [15].

Fig. 14(A.2 and B.2) aims to study the effect of feed concentration during the permeation study, where $ee_{L\text{-threonine}}$ (%) was obtained as 88 % for feed solution of 10 mmol.L^{-1}. Further, with an increase in the feed concentration, the conservation of probe chirality towards D-threonine

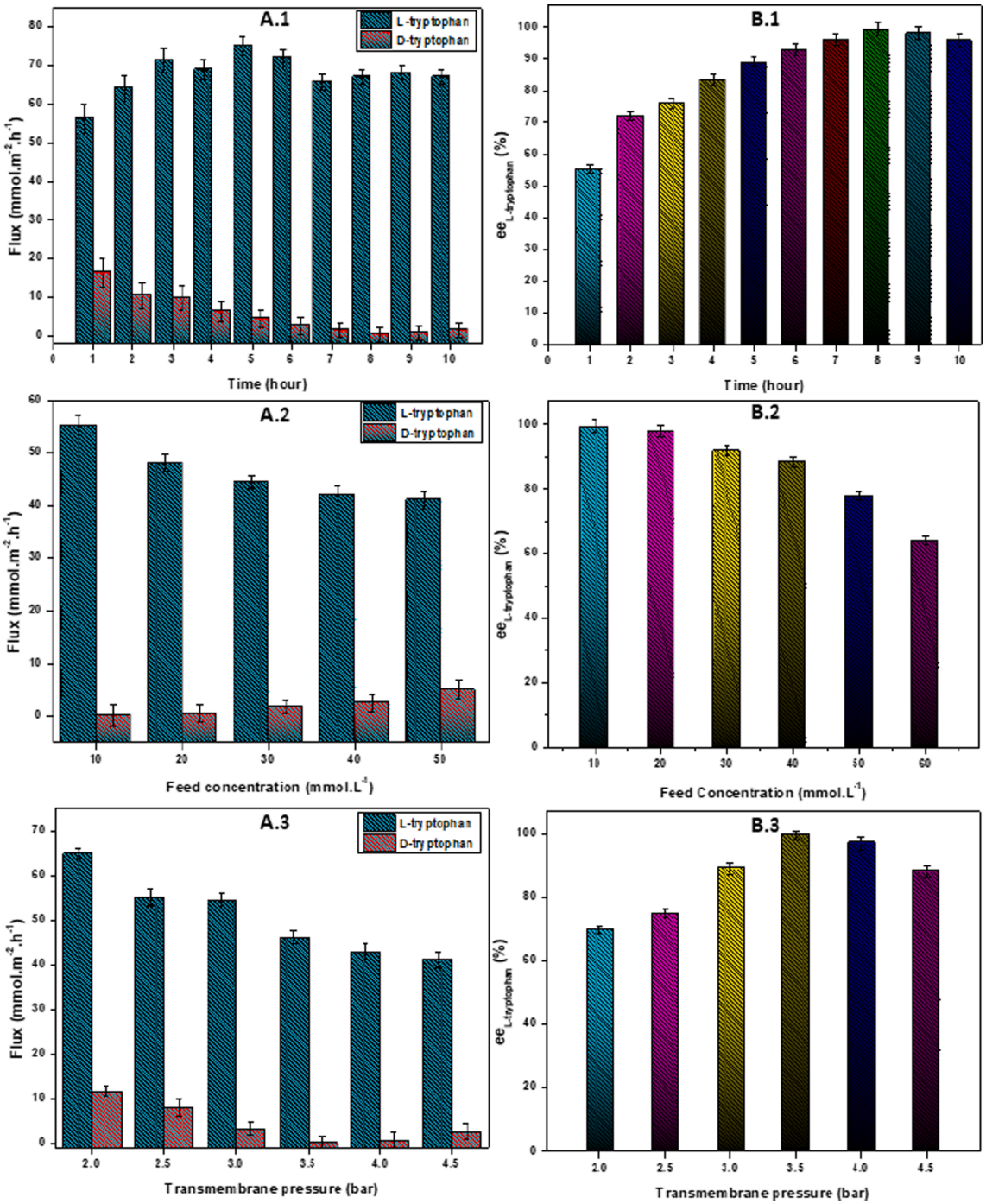

Fig. 15. Effect on DL-tryptophan upon membrane treatment in terms of (A) flux (B) $ee_{L\text{-threonine}}$ (%) values (A.1 and B.1) Change in permeation time; (A.2 and B.2) Change in feed concentration; (A.3 and B.3) Change in operating pressure at a constant flow rate of 25 mL.$min^{-1}$and temperature of 25 °C.

is observed, in which flux value increases from 3.01 to 6.68 mmol.m^{-2}.h^{-1} [14,15]. Moreover, its antipode represented a decrease in flux value from 47 to 38.41 mmol.m^{-2}.h^{-1} throughout its permeation study. The $ee_{L\text{-threonine}}$ (%) value was decreased and obtained at 70.34 % upon increasing the feed concentration beyond 10 mmol.L^{-1}.

The enantiomeric separation of threonine was also observed through variation of transmembrane pressure, which can evaluate the membrane performance based on flux and its enantiomeric excess. During membrane permeation, the membrane flux for both isomers of threonine is inverse with membrane pressure and tends to achieve consistency upon increased pressure [24]. The maximum $ee_{L\text{-threonine}}$ (%) value of 88.9 % was observed at a pressure of 3.5 bar, as shown in Fig. 14(B.3). This transmembrane pressure is obtained as optimum pressure. Upon further increasing the pressure, the $ee_{L\text{-threonine}}$ (%) value declined to 71.45 %.

The variation of membrane flux for racemic tryptophan is studied with respect to time also. The direct increase of flux for L-isomer was observed from 56.14 to 67 mmol.m^{-2}.h^{-1}, while D-isomer evaluated its contrapositive effect from 16.21 to 1.36 mmol.m^{-2}.h^{-1} as shown in Fig. 15(A.1 and B.1). Gradually, membrane flux values have reached a point of saturation. While $ee_{L\text{-tryptophan}}$ (%) increases from 55.17 % to 99.4 % during 8 h of membrane permeation due to its significant attraction with amide, whose reactivity gradually decreases due to its agglomeration within the membrane and therefore, the consistency was appeared in $ee_{L\text{-tryptophan}}$ (%).

In Fig. 15(A.2 and B.2), the change in membrane flux and $ee_{L\text{-tryptophan}}$ (%) with feed concentration of the solution resoluted the racemic tryptophan. The flux value gradually decreases and is optimized for L-tryptophan at 10 mmol.L^{-1} of a racemic solution; with further increment, the membrane flux gets saturated and $ee_{L\text{-tryptophan}}$ (%) value decreases to 64 %. The interaction of D-isomer with chiral probe showed an increase in flux from 0.16 to 8.78 mmol.m^{-2}.h^{-1} and it can pass through the porous membrane, whereas a consistent decrease was observed for L-tryptophan, from 55.19 to 40.04 mmol.m^{-2}.h^{-1} throughout the permeation experiment.

With an increase in *trans*-membrane pressure, the membrane flux of both D- and L- tryptophan decreases and gradually, it tends to achieve consistency. This consistency was determined by the pressure of 4 bar as shown in Fig. 15(A.3). Moreover, the enantiomeric excess of L-tryptophan also increases with increased pressure. Its maximum was obtained at 99.4 % under operating pressure of 3.5 bar, which decreases to 88.3 % due to concentration polarization within the membrane surface [14,15].

3.4. Selectivity versus molecular structure

The selectivity of the membrane in terms of enantiomeric excess can be explained from the molecular structure of the compounds as shown in Fig. 16. Depending upon their skeletal structure, a number of factors may be considered, including pi-pi stacking, aromatic stabilization of ring fragments, the inductive effect of adjacent groups, the presence of chiral center, and orientation of groups [26–27]. Membrane permeation experiments have revealed that tryptophan showed the highest enantiomeric excess value (~99.4%) compared to the other molecules. This is because tryptophan has an aromatic benzene structure adjacent to the indole ring, which exhibited a higher % ee for its L-isomer due to its self-association interaction between the D-isomer and the chiral probe. 1-methyltryptophan revealed 99.2% of enantiomeric excess because of its structural orientation. Due to the increase in ring current on heterocyclic ring of 1-methyl-tryptophan due to the CH_3 attached to it, the probable pi-pi stacking within pillared FSWCNT becomes probable highly effective. This can cause the isomeric resolution of its racemate effectively. Therefore, its L-isomer is rejected effectively through the membrane surface. Moreover, two hydroxyl groups on DOPA contributed higher enantiomeric excess (~98.9%) compared to tyrosine (~99%), having one hydroxyl group. However, available reactive groups present over ring fragments can cause more or less structural stability despite being bulky. Therefore, consideration of structural interaction of compounds through pillared FSWCNT and rGO appears to be more significant than steric crowding of ring compounds. Here, our primary focus contributes to the chiral center of the molecules, which is readily available in their long alkyl chain. Threonine has an acyclic carbon chain with a chiral center adjacent to the COOH group. Its reactivity towards the chiral probe is comparatively less and therefore, its enantiomeric excess value is the lowest. Since all the molecules have a chiral center and other reactive sites in their skeletal framework, there is a slight deviation in the enantiomeric excess of all compounds.

3.5. Mechanism behind the separation process

The membrane-based separation of chiral isomers can be supported by one of the most suitable mechanisms reported by Easson-Stedman, which is known as the “three-point interaction” model [28]. The mechanism states that the interaction between chiral probe and one of the enantiomers involves at least three interaction sites. The discrimination of the other enantiomer becomes readily available. This model is in accordance with the fact that one enantiomer should have two non-

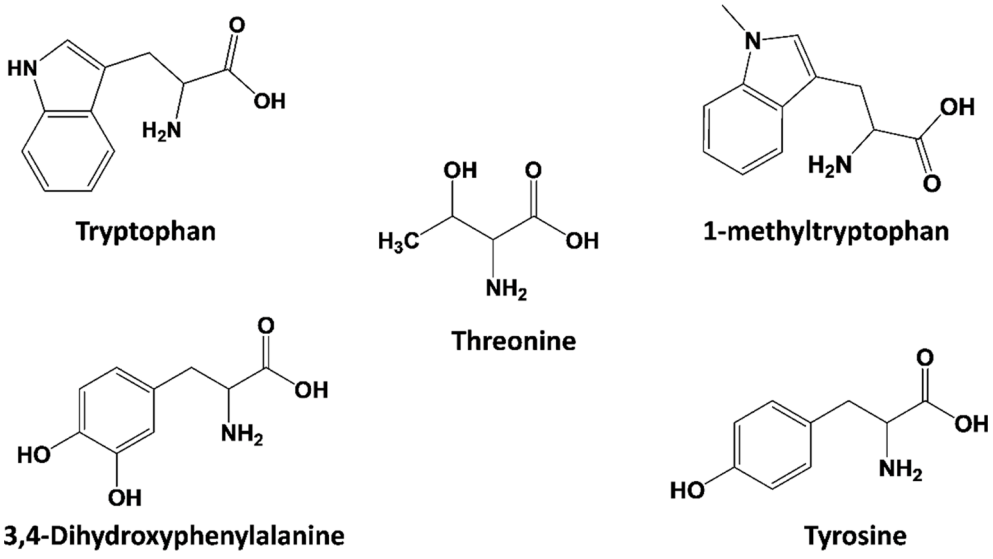

Fig. 16. Chemical structure of β-substituted-α-amino acids.

bonding hydrogen bonds and one $\pi - \pi$ interaction. In contrast, the other should have only two interactions due to their configurational change. The enantiomer with more vital interaction with chiral probe will firmly retain over the membrane surface, whereas the other will easily permeate through the available porous channel [29–31]. The plausible reversible complexation between enantiomers and chiral recognition sites involves H-bonding, electrostatic interactions, etc. [15]. Although diffusion and convection are both selective mechanisms during the separation process, the chiral separation process is mainly based on the diffusion process principle. In our case, the preferred L–isomer may preferentially diffuse into the void space in the polymeric matrix, whereas the counter isomer will get adsorbed with a higher rate followed by the convective flow. The polymeric membrane surface may exhibit both diffusions selective or sorption selective behavior during the enantiomeric separation process [32].

4. Conclusion

Our research work firmly established the interaction between chiral probes and selectors within the pillared network form on the separation behavior of novel membrane. The composite was introduced onto the raw PSf support by vertically aligned carbon nanotube within graphene sheets. Thermal stability of membranes was achieved at a maximum temperature of 610 °C. Further, the performance of the chiral membrane was determined by continuous membrane permeation for separation of β-substituted-α-amino acids *viz* 3,4-Dihydroxyphenylalanine, Tryptophan, Threonine, Tyrosine and 1-methyltryptophan. Results demonstrate that rGO-FSWCNT membranes have higher membrane flux towards D-enantiomers than L-enantiomers and thus yield stereospecific enantioselectivity. The highest enantiomeric excess of 99.4% for DL-tryptophan was obtained under the optimized concentration of rGO-FSWCNT as 3 % in the membrane, *trans*-membrane pressure of 3.5 bar, feed concentration of less than 10 mmol.L^{-1} at a temperature of 35 °C. The mechanical strength and surface roughness of membranes were remarkably affected through the addition of rGO-FSWCNT. Therefore, membrane flux for L-isomer gradually increases. These were attributed to the introduction of rGO-FSWCNT composite, which can act as a reactive site to improve the performance of chiral selectors and, therefore, enhance the enantioselectivity. Our obtained results suggest that introducing FSWCNT into the GO sheets provides the potential to implement higher enantioselectivities in the membrane-based treatment of racemic compounds.

CRediT authorship contribution statement

Monti Gogoi: Methodology, Software, Formal analysis, Investigation, Resources, Data curation, Writing – original draft, Writing – review & editing. **Rajiv Goswami:** Software, Writing – original draft. **Alimpia Borah:** Formal analysis, Investigation, Resources, Data curation, Writing – original draft. **Swapnali Hazarika:** Conceptualization, Visualization, Methodology, Validation, Writing – review & editing, Supervision, Project administration, Funding acquisition.

Declaration of Competing Interest

The authors declare that they have no known competing financial interests or personal relationships that could have appeared to influence the work reported in this paper.

Acknowledgment

The authors gratefully acknowledge Dr G Narahari Sastry, Director, CSIR-NEIST, for encouraging the research group to carry out this work. The authors would also like to acknowledge CSIR, New Delhi for funding the research work.

Appendix A. Supplementary material

Supplementary data to this article can be found online at https://doi.org/10.1016/j.seppur.2021.120201.

References

[1] R. Xie, L.Y. Chu, J.G. Deng, Membrane and membrane processes for chiral resolution, Chem. Soc. Rev. 37 (2008) 1243–1263.
[2] A. Higuchi, M. Tamai, Y.-A. Ko, Y.-I. Tagawa, Y.-H. Wu, B.D. Freeman, J.-T. Bing, Y. Chang, Q.-D. Ling, Polymeric membranes for chiral separation of pharmaceuticals and chemicals, Polym. Rev. 50 (2) (2010) 113–143.
[3] S.-Y. Zhang, C.-X. Yang, W. Shi, X.-P. Yan, P. Cheng, L. Wojtas, M.J. Zaworotko, A Chiral Metal-Organic Material that Enables Enantiomeric Identification and Purification, Chem 3 (2) (2017) 281–289.
[4] I. Weissbuch, M. Lahav, Crystalline Architectures as Templates of Relevance to the Origins of Homochirality, Chem. Rev. 111 (5) (2011) 3236–3267.
[5] D. Hirose, A. Isobe, E. Quiñoá, F. Freire, K. Maeda, Three-State Switchable Chiral Stationary Phase Based on Helicity Control of an Optically Active Poly (phenylacetylene) Derivative by Using Metal Cations in the Solid State, J. Am. Chem. Soc. 141 (21) (2019) 8592–8598.
[6] F. Zhang, Y. Sun, D. Tian, H. Li, Chiral Selective Transport of Proteins by Cysteine-Enantiomer-Modified Nanopores, Angew. Chem. Int. Ed. 56 (25) (2017) 7186–7190.
[7] Y. WANG, Y. HU, J. XU, G. LUO, Y. DAI, Immobilization of lipase with a special microstructure in composite hydrophilic CA/hydrophobic PTFE membrane for the chiral separation of racemic ibuprofen, J. Membr. Sci. 293 (1-2) (2007) 133–141.
[8] J. Shen, Y. Okamoto, Efficient separation of enantiomers using stereoregular chiral polymers, Chem. Rev. 116 (3) (2016) 1094–1138.
[9] J. Hu, W.G. Cochrane, A.X. Jones, D.G. Blackmond, B.M. Paegel, Chiral lipid bilayers are enantioselectively permeable, Nature Chem. 13 (8) (2021) 786–791.
[10] C.A.M. Afonso, J.G. Crespo, Recent advances in chiral resolution through membrane-based approaches, Angew. Chem. Int. Ed. 43 (40) (2004) 5293–5295.
[11] Y. Lu, H. Zhang, J.Y. Chan, R. Ou, H. Zhu, M. Forsyth, E.M. Marijanovic, C. M. Doherty, P.J. Marriott, M.M.B. Holl, H. Wang, Homochiral MOF-Polymer Mixed Matrix Membranes for Efficient Separation of Chiral Molecules, Angew. Chem. Int. Ed. 58 (47) (2019) 16928–16935.
[12] C. Meng, Y. Sheng, Q. Chen, H. Tan, H. Liu, Exceptional chiral separation of amino acid modified graphene oxide membranes with high-flux, J. Membr. Sci. 526 (2017) 25–31.
[13] E.J. Son, S.H. Lee, S.K. Kuk, M. Pesic, D.S. Choi, J.W. Ko, K. Kim, F. Hollmann, C. B. Park, Carbon Nanotube-Graphitic Carbon Nitride Hybrid Films for Flavoenzyme-Catalyzed Photoelectrochemical Cells, Adv. Funct. Mater. 28 (24) (2018) 1705232.
[14] M. Gogoi, R. Goswami, P.G. Ingole, S. Hazarika, Selective permeation of L-tyrosine through functionalized single-walled carbon nanotube thin-film nanocomposite membrane, Sep. Purif. Technol. 233 (2020) 116061.
[15] M. Gogoi, R. Goswami, A. Borah, H. Sarmah, P. Rajguru, S. Hazarika, Amide functionalized DWCNT nanocomposite membrane for chiral separation of the racemic DOPA, Sep. Purif. Technol. 279 (2021), 119704.
[16] A. Gogoi, T.J. Konch, K. Raidongia, K. Anki Reddy, Water and salt dynamics in multilayer graphene oxide (GO) membrane: Role of lateral sheet dimensions, J. Membr. Sci. 563 (2018) 785–793.
[17] T.J. Konch, R.K. Gogoi, A. Gogoi, K. Saha, J. Deka, K.A. Reddy, K. Raidongia, Nanofluidic transport through humic acid modified graphene oxide nanochannels, Mater. Chem. Front. 2 (9) (2018) 1647–1654.
[18] C. Meng, Q. Chen, H. Tan, Y. Sheng, H. Liu, Role of filled PLGA in improving enantioselectivity of Glu-GO/PLGA composite membranes, J. Membr. Sci. 555 (2018) 398–406.
[19] N.I. Zaaba, K.L. Foo, U. Hashim, S.J. Tan, W. Liu, C.H. Voon, Synthesis of graphene oxide using modified hummers method: solvent influence, Sci. Technol. Humanit. 184 (2017) 469–477.
[20] O. Choi, S. Karki, R.R. Pawar, S. Hazarika, P.G. Ingole, A new perspective of functionalized MWCNT incorporated thin film nanocomposite hollow fiber membranes for the separation of various gases, J. Environ. Chem. Eng. 9 (1) (2021) 104774, https://doi.org/10.1016/j.jece:2020.104774.
[21] R. Goswami, M. Gogoi, A. Borah, H. Sarmah, P.G. Ingole, S. Hazarika, functionalized activated carbon and carbon nanotube hybrid membrane with enhanced antifouling activity for removal of cationic dyes from aqueous solution, Environ. Nanotechnol. Monitoring Manage. 16 (2021) 100492, https://doi.org/10.1016/j.enmm.2021.100492.
[22] P. Saikia, K. Dutta, A.K. Guha, S.K. Dolui, P. Barman, L.J. Borthakur, High-performance aqueous electrolyte based supercapacitor of carboxylic acid functionalized carbon-nanotubes and graphene nano composite, Mater. Chem. Phy. 258 (2021) 123786.
[23] R. Goswami, M. Gogoi, H.J. Borah, P.G. Ingole, S. Hazarika, Biogenic synthesized Pd-nanoparticle incorporated antifouling polymeric membrane for removal of crystal violet dye, J. Environ. Chem. Eng. 6 (5) (2018) 6139–6146.
[24] S. Hazarika, Enantioselective permeation of racemic alcohol through polymeric membrane, J. Membr. Sci. 310 (1-2) (2008) 174–183.
[25] H. Wu, B. Tang, P. Wu, MWNTs/polyester thin film nanocomposite membrane: an approach to overcome the trade-off effect between permeability and selectivity, J. Phys. Chem. C 114 (39) (2010) 16395–16400.

[26] R. Carrillo, M. Lopez-Rodriguez, V.S. Martin, T. Martin, Quantification of a CH–π Interaction Responsible for Chiral Discrimination and Evaluation of Its Contribution to Enantioselectivity, Angew. Chem. 121 (2009) 7943–7948.
[27] K. Saigo, Y. Kobayashi, The Role of CH/π Interaction in the Stabilization of Less-Soluble Diastereomeric Salt Crystals, Chem.Record 7 (2007) 47.
[28] L.H. Easson, E. Stedman, Studies on the Relationship Between Chemical Constitution and Physiological Action: Molecular Dissymmetry and Physiological Activity, Biochem. J. 27 (1933) 1257–1266.
[29] W.H. Pirkle, T.C. Pochapsky, Considerations of chiral recognition relevant to the liquid chromatography separation of enantiomers, Chem. Rev. 89 (2) (1989) 347–362.
[30] V.A. Davankov, V.R. Meyer, M. Rais, A vivid model illustrating chiral recognition induced by achiral structures, Chirality 2 (4) (1990) 208–210.
[31] V.A. Davankov, The nature of chiral recognition: Is it a three-point interaction? Chirality 9 (1997) 99–102.
[32] A. Higuchi, M. Tamai, Y.-A. Ko, Y.-I. Tagawa, Y.-H. Wu, B.D. Freeman, J.-T. Bing, Y. Chang, Q.-D. Ling, Polymeric Membranes for Chiral Separation of Pharmaceuticals and Chemicals, Polym. Rev. 50 (2) (2010) 113–143.